

High-Efficiency Dye-Sensitized Solar Cell with Three-Dimensional Photoanode

Nicolas Tétreault,^{*,†} Éric Arsenault,[‡] Leo-Philipp Heiniger,[†] Navid Soheilnia,[‡] Jérémie Brillet,[†] Thomas Moehl,[†] Shaik Zakeeruddin,[†] Geoffrey A. Ozin,^{*,‡} and Michael Grätzel[†]

[†]Laboratory of Photonic and Interfaces, Institute of Physical Chemistry, École Polytechnique Fédérale de Lausanne, 1015 Lausanne, Switzerland

[‡]Materials Chemistry and Nanochemistry Research Group, Center for Inorganic and Polymeric Nanomaterials, Department of Chemistry, University of Toronto, 80 St. George Street, Toronto, Ontario M5S 3H6, Canada

 Supporting Information

ABSTRACT: Herein, we present a straightforward bottom-up synthesis of a high electron mobility and highly light scattering macroporous photoanode for dye-sensitized solar cells. The dense three-dimensional Al/ZnO, SnO₂, or TiO₂ host integrates a conformal passivation thin film to reduce recombination and a large surface-area mesoporous anatase guest for high dye loading. This novel photoanode is designed to improve the charge extraction resulting in higher fill factor and photovoltage for DSCs. An increase in photovoltage of up to 110 mV over state-of-the-art DSC is demonstrated.

KEYWORDS: Photovoltaic devices, dye-sensitized solar cells, host–guest, self-assembly, transparent conductive oxides



Dye-sensitized solar cells (DSCs) are one of the most promising photovoltaic technologies for production of renewable, clean, and affordable energy. They are generally made from cheap and nontoxic components and can be designed in a variety of different colors and transparencies, which distinguishes them as an ideal photovoltaic concept for integrated “green” architecture. Additionally, they have been shown to be competitive with other thin film technologies reaching certified efficiencies as high as 11.1% when using a triiodide/iodide (I_3^-/I^-) redox shuttle.^{1–3}

In DSCs, charge carrier generation takes place in a chemisorbed monolayer of photoactive dye that is sandwiched between a semiconducting oxide, usually anatase TiO₂, and an electrolyte acting as electron and hole conducting materials, respectively. Because of the relatively low-absorption cross-section of the molecular sensitizer, a high surface area mesoscopic photoanode is necessary to ensure high dye loading and efficient light harvesting in the visible part of the solar spectrum. This implies that the DSC has an exceedingly large, heterogeneous interface through which electrons may be (parasitically) intercepted as a result of the slow electron transport. The latter is governed by an ambipolar diffusion mechanism controlled by trap-limited hopping through a relatively long and tortuous path to the transparent conductive electrode.^{4–7} It is further hindered by the low electron mobility in anatase TiO₂ nanoparticles and the multiple grain boundaries in the mesoporous film.⁸

Given a charge collection time of milliseconds at the maximum power point,⁹ efficient charge extraction is only made possible when using the (I_3^-/I^-) redox couple through the slow interception

of electrons by adjacent I_3^- .¹⁰ In addition to limited light harvesting by the dye, one of the main limiting factors of efficiency is the excessive driving force of 0.6 eV necessary for the dye-regeneration process leading to a significant loss-in-voltage of approximately 600 mV.^{7,11,12} This has sparked development and study of various alternative redox couples including p-type semiconductors.¹³ Increasingly, development has been centered around the use of organic hole-transporting materials (HTM) in solid-state DSCs (ss-DSCs).^{14–17}

The electronic loss that is typically discussed for DSCs is slow transport-induced recombination.^{18–21} If charges recombine before reaching the electrode then this has a direct influence on the photocurrent and photovoltage. The open-circuit voltage is defined by the splitting of the quasi-Fermi level of electrons in the metal oxide and the redox potential of the electrolyte (quasi-Fermi level of holes in the hole-transporter). Hence, the closer the Fermi level in the metal oxide can be pushed toward the conduction band and LUMO level of the sensitizer, the higher the open-circuit voltage, and the smaller the loss-in-potential going from the level of the excited state of the dye to the quasi-Fermi level in the metal oxide. Two strategies can contribute to this upward shift and increase the open-circuit potential, namely reducing the recombination rate constant enabling the Fermi level to move closer to the conduction band before the recombination

Received: May 26, 2011

Revised: September 25, 2011

Published: September 30, 2011

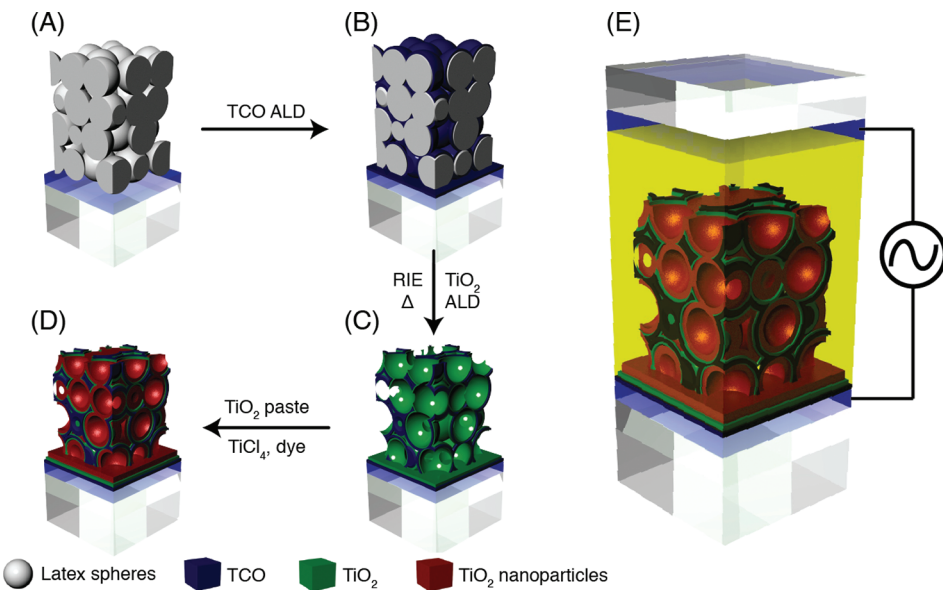


Figure 1. Schematic representation of the synthesis method for a 3D host–guest dye-sensitized solar cell. (A) Doctor-bladed, disordered template of 2.2 μm polystyrene spheres. (B) Layer-by-layer conformal deposition of the host material (Al/ZnO , TiO_2) by ALD. (C) After RIE to open the top surface, the template is removed by annealing at 360 °C to reveal a disordered inverse opal of host material. It is then conformally coated with 25 nm of dense TiO_2 by ALD. (D) Pore filling with high surface area nanocrystalline TiO_2 and dye loading. (E) Liquid electrolyte infiltration and sealing of the dye sensitized solar cell.

rate balances the charge generation rate or shifting the conduction band itself. Finally, enhancing the electron transport could improve charge collection and reduce IR losses, enhance the short-circuit current, and fill factor.^{12,18}

Several approaches have been proposed in order to reduce interfacial recombination and improve charge collection in liquid electrolytes and ss-DSCs including the use of radial collection nanostructures,⁷ one-dimensional ZnO and TiO_2 nanorods, and nanowires as photoanodes.^{22–25} Even though these approaches show great promise, they have yet to achieve power conversion efficiencies above 5% in liquid electrolyte DSCs and 1.7% in ss-DSCs. Lately, we were able to show faster electron transport using a novel three-dimensional (3D) self-assembled anatase TiO_2 fibrous network photoanode capable of enhanced light harvesting and charge transport to reach an efficiency of 5%, a record for nanowire-based ss-DSCs.²⁶

Particular attention has been given to ZnO and SnO_2 as alternatives to TiO_2 in DSCs due to their higher electronic conductivity and electron mobility when compared to TiO_2 .²⁷ Despite faster electron transport,²⁷ only rather poor device efficiencies have been reported to date for DSCs employing nanocrystalline SnO_2 .^{7,23,28–30} In part, this was found to be due to a 2–3 orders of magnitude increase in the recombination rates when the high mobility material is in direct contact with the sensitizer and/or the electrolyte.²⁷ This finding led to a host of publications on the addition of blocking (passivating) layers covering the ZnO or SnO_2 in order to reduce this recombination rate resulting in higher photovoltage.^{7,31,32}

Herein, we demonstrate a novel bottom-up 3D host–passivation–guest (H-P-G) electrode concept that enables structural control on the electron extraction, conduction band, and the recombination dynamics as well as on the optical scattering in photovoltaic devices. This new type of electrode is exemplified herein by incorporating it into a DSC photoanode to significantly improve photocurrent, fill factor, and most importantly the

photovoltage. This is shown through a strong decrease in dark current when comparing a 3D TiO_2 host to high electron mobility Al/ZnO and SnO_2 hosts. To ensure high dye loading, the macropores contained in the passivated 3D host are infiltrated with anatase TiO_2 nanoparticles to form a conformal mesoporous film enabling optimized sensitization and electron injection characteristics found in traditional nanoparticle-based DSCs. Using this novel architecture, an increase in the photovoltage of up to 110 mV over state-of-the-art TiO_2 , ZnO, and SnO_2 -based DSCs is obtained. The straightforward and simple bottom-up fabrication technique produces a highly optically scattering photoanode that could enable enhanced light harvesting,¹ fast charge extraction, reduced interfacial recombination, and lower IR loss to significantly increase the cell photovoltage, photocurrent, and the fill factor.¹² The concept electrode is well suited for DSCs since only a small volume fraction is lost to the optically inactive 3D host material leaving most of the volume for the light harvesting sensitized nanoparticle TiO_2 mesoporous film.

A schematic representation of the intermediate materials involved in the fabrication of a 3D H-P-G photoanode for DSCs is shown in Figure 1. The overall fabrication method is inspired by micromolding in inverse opals (MISO) first developed for the synthesis of large-area oxide inverse opals and then extended for high-temperature fabrication of full-photonic bandgap semiconductor photonic crystals from polymer templates.^{33,34} In particular, a dispersion of polystyrene macrospheres in isopropanol is used to accelerate the capillary force-induced self-assembly of the polystyrene macrospheres ($\Phi = 2.2 \mu\text{m}$) and thereby obtain a highly disordered opal template of uniform thickness. Using large monodispersed spheres enables the formation of a uniform template with predictably large interconnecting pores extending in all three spatial dimensions. The thickness of the template is adjusted through the volume concentration of spheres in the isopropanol dispersion (~22 vol % for 10–12 μm thick template film).

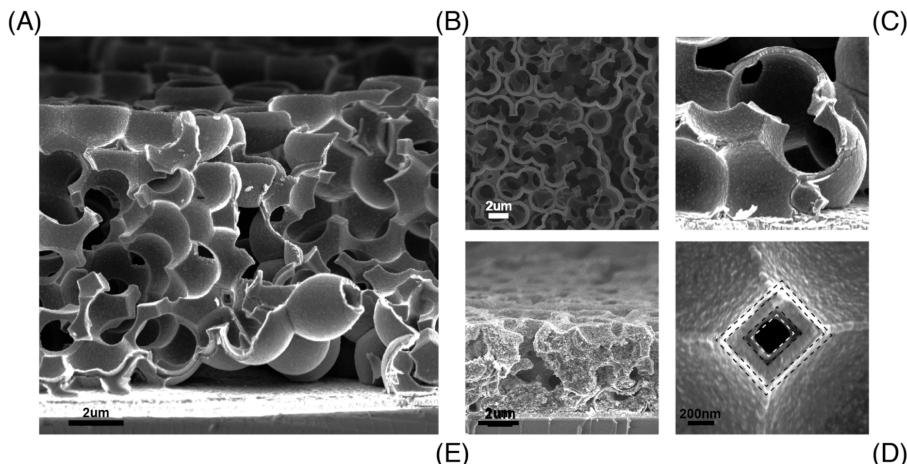


Figure 2. Scanning electron micrograph of a self-assembled 3D Al/ZnO | TiO₂ host–guest dyes-sensitized solar cell photoanode. (A) Cross-sectional view of a disordered TiO₂ passivated 3D Al/ZnO backbone. (B) Top-view of the 3D macroporous Al/ZnO after top surface removal by reactive ion etching and template removal by annealing. (C) High-magnification micrograph showing the TiO₂ covered 3D macroporous Al/ZnO host in direct contact with the front FTO electrode. (D) High-magnification micrograph showing the 3D Al/ZnO conformally coated with a 25 nm thin film of dense TiO₂ inside and out. (E) Complete photoanode after infiltration and calcination of the TiO₂ nanoparticle paste.

The dispersion is then doctor bladed, a scalable fabrication technique, on a transparent conductive FTO-covered glass substrate to reveal a large-area highly light scattering disordered template (Figure 1a). It is then heated and infiltrated with 90 nm of Al/ZnO (1:9), SnO₂, or TiO₂ in a highly conformal fashion by atomic layer deposition (ALD) by alternating pulses of organometallic precursors and hydrolytic polycondensation agent (H₂O) in exposure mode (Figure 1b). Recently ALD has been gaining interest as a powerful research tool for creating highly conformal layers on nanostructured electrodes³⁵ and has even been used for surface state passivation of TiO₂ in dye sensitized solar cells and Fe₂O₃ in photolysis.^{36,37} The deposition temperature is optimized to increase the template interconnecting pore size by softening of the polymer beads ensuring proper sphere necking.³⁸ Large interconnecting pores between spheres will enable proper filling with the guest nanocrystalline TiO₂ later on. A quick dry reactive ion etching (RIE) of the infiltrated opal's top surface oxide is performed before removing the polymer template by annealing (360 °C, 15 min.) We thus obtain a 3D host backbone that is well connected to the underlying FTO–glass front electrode. The direct electronic connection will ensure efficient charge extraction throughout the interconnected 3D H-P-G electrode. The surfaces of the TCO backbone are then conformally coated with 25 nm of dense TiO₂ by ALD in order to reduce interfacial recombination between electrons in the highly conducting TCO backbone and the I₃⁻ oxidized electrolyte (Figure 1c).²⁷ After calcination (500 °C, 15 min.) the hexagonal wurtzite, cassiterite, and anatase crystal structures of the Al/ZnO, SnO₂, and TiO₂, respectively, were confirmed by powder X-ray diffraction (see Supporting Information, Figure S1). In order to provide enough surface area for dye sensitization and efficient light harvesting, the macroporous inverse TCO backbone is infiltrated by sequential doctor-blading of a low viscosity 17 nm anatase nanocrystal paste (Figure 1d).

Scanning electron micrographs (SEM) of a 3D Al/ZnO | TiO₂ anatase nanoparticles H-P-G photoanode are presented in Figure 2. The cross-sectional and top view (Al/ZnO host) micrographs (Figure 2a,b) clearly show the high pore connectivity throughout the 3D open structure as well as the significant

disorder inherited from the polystyrene template. From these micrographs, we can conclude that the backbone only uses a small volume fraction of the 3D film (~10%). This is an additional advantage of the 3D macroporous structure where the high degree of necking between the templating spheres and the very thin (90 nm) film of metal oxide host deposited leave the vast majority of the volume for filling with the guest material. The macroporous structure further enables the conformal coating of the 3D host on both sides with dense TiO₂ by ALD (Figure 2c,d). The role of the TiO₂ overlayer is to passivate the TCO surface to improve its chemical stability and further reduce recombination rate at the conductive transparent oxide - electrolyte interface. Visible in Figure 2c is the direct contact between the 3D host and the FTO–glass that will ensure unhindered electron transfer from the 3D host–guest structure and the front DSC electrode. Additionally, subsequent TiO₂ deposition was found to cover the FTO in addition to the 3D host to effectively block recombination at the FTO–electrolyte interface. Figure 2e shows the 3D Al/ZnO | TiO₂ anatase nanoparticles H-P-G electrode after partial filling with mesoporous anatase to constitute the finished 3D TCO photoanode. We estimate from SEM pictures that about 50% on the internal volume is filled with the anatase TiO₂ nanoparticles. The disordered structure and the partial filling at the scale of light combine to induce high optical scattering in the 3D H-P-G structure (see Supporting Information, Figure S2)

Complete DSC devices were prepared using 10–12 μm thick 3D TiO₂ | TiO₂ anatase nanoparticles, Al/ZnO | TiO₂ anatase nanoparticles and SnO₂ | TiO₂ anatase nanoparticles H-P-G photoanodes on a FTO–glass substrate. In both cases, 90 nm of the host and 25 nm of TiO₂ were deposited by ALD for a maximum wall thickness of 140 nm. Each of the macroporous 3D H-P-G structures were partially filled with a 17 nm anatase nanoparticle paste using a modified doctor blading procedure. Individual infiltrations were separated by 10 min heating at 120 °C to ensure solvent evaporation and densification of the conformal paste thin film. The electrode is then calcined to burn off the organic materials found in the paste (500 °C, 60 min, 2 °C/min ramp).³⁹ In order to improve the anatase nanoparticle

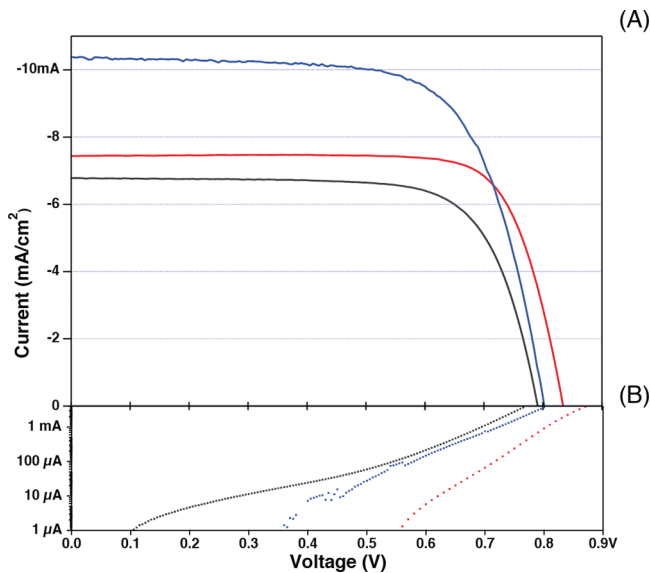


Figure 3. Photocurrent density–voltage (J – V) characteristics of the 3D host–passivation–guest dye-sensitized solar cells under AM 1.5 illumination and in the dark. Solid (A) and dashed (B) lines represent the current under standard illumination and in the dark, respectively, for Al/ZnO (red, $J_{sc} = 7.5 \text{ mA}/\text{cm}^2$, $V_{oc} = 842 \text{ mV}$, ff = 0.77, $\eta = 4.9\%$), SnO₂ (blue, $J_{sc} = 10.4 \text{ mA}/\text{cm}^2$, $V_{oc} = 803 \text{ mV}$, ff = 0.70, $\eta = 5.8\%$) and TiO₂ (black, $J_{sc} = 6.9 \text{ mA}/\text{cm}^2$, $V_{oc} = 791 \text{ mV}$, ff = 0.73, $\eta = 4.0\%$) hosts.

connectivity and increase the photocurrent, the TiO₂ and SnO₂ H-P-G photoanodes were immersed into a 40 mM aqueous TiCl₄ solution at 70 °C for 30 min and washed with water and ethanol.³⁹ This treatment could not be done on the Al/ZnO-based electrode since it is not chemically stable enough to sustain immersion in strong acid at elevated temperature. We should thus expect a penalty on the photocurrent for this photoanode.

The films are sintered for 30 min at 500 °C before dipping in a 0.3 mM Z907 solution for 10 min. Z907 has been supplanted recently by ruthenium and organic dyes with higher molar coefficient but we were willing to sacrifice some photocurrent in exchange for high versatility and well-characterized photovoltaic characteristics enabling a direct comparison with published data (Z907: $J_{sc} = 17.13 \text{ mA}/\text{cm}^2$, $V_{oc} = 730 \text{ mV}$, ff = 0.724, $\eta = 9.05\%$).⁴⁰ Following the immersion procedure, the dye-sensitized electrodes were rinsed with acetonitrile and dried in air. The photoanodes are then assembled using a thermally platinized FTO (TEC15) counter electrode using a 25 μm thick hot melt ring and sealed by heating. The cell internal space was filled with a I₃⁻/I⁻ electrolyte in a 85:15 acetonitrile/valeronitrile mixture.

Shown in Figure 3a are the J – V characteristics for the dye-sensitized solar cells based on TiO₂, SnO₂, and Al/ZnO 3D host photoanodes. We find an increase in short-circuit current density going from a TiO₂ ($J_{sc} = 6.9 \text{ mA}/\text{cm}^2$) to Al/ZnO ($J_{sc} = 7.9 \text{ mA}/\text{cm}^2$) and SnO₂ ($J_{sc} = 10.4 \text{ mA}/\text{cm}^2$). The photocurrent for the Al/ZnO host is found to be significantly lower than that of SnO₂ because of the lack of TiCl₄ treatment on the former. This treatment enhances connectivity between anatase TiO₂ nanoparticles to significantly increase the photocurrent and photovoltage in state-of-the-art DSCs by improving electron hopping at the anatase nanoparticle boundaries.⁴¹ Even though the Al/ZnO host is protected by TiO₂ it is impossible to ensure a complete, pinhole free protection against the low pH TiCl₄

solution. It is possible that the increase in photocurrent observed is a direct consequence of the high electron mobility in the Al/ZnO and SnO₂ hosts (241 and 16.5 cm²/(V s), respectively), which is 5–6 orders of magnitude higher than measured for anatase TiO₂ nanoparticles at high voltage ($V = 0.8 \text{ V}$, $2.30 \times 10^{-4} \text{ cm}^2/(\text{V s})$) (see Supporting Information, Table S1).⁸ In addition, the fill factor is found to be greater for the Al/ZnO (ff = 0.77) host than for the TiO₂ (ff = 0.73) host. Regardless of the host material, the 3D H-P-G photoanodes all present photovoltages well above the $V_{oc} = 730 \text{ mV}$ obtained with the best performing Z907 DSCs.⁴⁰ Indeed, an improvement of 60 and 110 mV for TiO₂ ($V_{oc} = 791 \text{ mV}$) and Al/ZnO ($V_{oc} = 842 \text{ mV}$) hosts are obtained, respectively. A significant increase in photovoltage is to be expected when reducing the dark current which depends on the conduction band position and recombination dynamics in the cell. Indeed, a significant decrease in the dark current is observed going from the TiO₂ to the Al/ZnO host as can be seen in 3b. Further variations in the J – V characteristics for two additional dye/coadsorbent configurations (Z907/GBA and N719) are presented in the Supporting Information Figure S3.

When compared to previous studies using high mobility materials like SnO₂ and ZnO passivated with TiO₂ in liquid electrolyte DSCs we find that the photovoltage obtained with the 3D host–guest photoanodes are higher by at least 90–100 mV.^{7,23,28–30} Additionally, an increase of about 60 and 110 mV over our published state-of-the-art values for Z907 dye and iodine-based volatile electrolyte is obtained for 3D TiO₂ and Al/ZnO hosts, respectively. One of the major advantages in using transparent high mobility materials, for example, ZnO and SnO₂, for charge injection and collection in DSCs lies in its relatively low transport resistance when compared to that of anatase TiO₂ nanoparticles.^{42–44} However, this advantage was found to be counterbalanced by faster electron recombination dynamics with the oxidized electrolyte via intrabandgap surface states ultimately limiting the efficiency of such cells.⁴⁴ This led to the study of various capping materials (Al₂O₃, TiO₂, MgO, etc.) that slow down recombination leading to increases in photocurrent and photovoltage.^{7,31,32} In addition to acting as an effective protection layer for the chemically unstable ZnO against the acidic dye solution,⁴⁵ the complete coverage of the host material with ALD of a dense 25 nm TiO₂ layer can passivate surface traps³⁷ and increase charge transfer resistance to the oxidized dye and electrolyte. This is clearly visible in the decrease in dark current observed (Figure 3b). According to the literature, this can be due to a decrease in recombination or a shift of the conduction band toward vacuum. Both would lead to a shift in the quasi-Fermi level with respect to the redox potential of the electrolyte and contribute to the significant increase in the observed photovoltage.⁷ These findings will motivate further mechanistic studies on the role of the various interfaces, conduction pathways, and electronic properties of the various materials that could induce band bending, affect injection dynamics, or shift the conduction band position.

In conclusion, we demonstrated a novel bottom-up 3D H-P-G DSC photoanode made of a high electron mobility host, a passivating conformal blocking layer and a high surface area guest to improve short circuit current density, fill factor, and photovoltage. The 3D H-P-G photoanode shows a strong decrease in dark current when using Al/ZnO with electron mobility and diffusion coefficient up to 6 orders of magnitude higher than that of anatase TiO₂ nanoparticles. By completely covering the 3D host with a dense passivating TiO₂ thin film and

filling its macropores with anatase nanoparticles, we ensure a high surface area for dye loading and maintain injection dynamics typical of anatase nanoparticle-based DSCs. Using this novel 3D H-P-G morphology partially filled with anatase nanoparticles, we show an increase in photovoltage of up to 110 mV over state-of-the-art TiO₂ and ZnO DSCs with Z907 and I₃⁻/I⁻ redox couple. The concept electrode is well suited for DSC since only a small volume fraction is lost to the transparent 3D host material leaving most of the volume for the light harvesting sensitized mesoporous anatase TiO₂. The straightforward and simple bottom-up fabrication technique produces a highly optically scattering 3D photoanode material that could enhance light harvesting and charge extraction and reduce interfacial recombination to significantly increase the cell photovoltage, photocurrent and the fill factor in various low cost photovoltaic technologies.⁴⁶

Methods. *Three-Dimensional Host–Passivation–Guest Photoanode Fabrication.* A 22 vol % dispersion of 2.2 μm polystyrene macrospheres in isopropanol is doctor bladed on a TEC15 FTO-covered glass substrate to reveal a large-area highly light scattering disordered template. It is then heated and infiltrated with 90 nm of Al/ZnO (1:9), SnO₂, or TiO₂ in a highly conformal fashion by atomic layer deposition (ALD) pulses of trimethylaluminum, diethylzinc and water (Al(Me)₃, Zn(Et)₂|H₂O, 114 °C, 1:9), tetrakis(dimethylamino)tin and ozone (Sn(NMe₂)₄|O₃, 200 °C) and tetrakis(dimethylamino)-titanium and water (Ti(NMe₂)₄|H₂O, 200 °C) using nitrogen as a carrier gas (Cambridge Nanotech Savannah S100). The infiltrated opal's top surface oxide is removed by RIE (6 min, 1800W, C₄F₈, Ar carrier gas, AMS200) performed before removing the polymer template by annealing (360 °C, 15 min.) The TCO backbone is then conformally coated with 25 nm of dense TiO₂ by ALD in order to reduce interfacial recombination between electrons in the highly conducting TCO backbone and the I₃⁻ oxidized electrolyte (Figure 1c).²⁷ The 3D H-P-G structures were filled with a 17 nm anatase nanoparticle paste through four sequential doctor blading separated by 10 min heating at 120 °C to ensure solvent evaporation and densification of the conformal paste thin film. The electrode is then calcined to burn off the organic materials found in the paste (500 °C, 60 min, 2 °C/min ramp).³⁹ In order to improve the anatase nanoparticle connectivity and increase the photocurrent, the TiO₂ and SnO₂ H-P-G photoanodes were immersed into a 40 mM aqueous TiCl₄ solution at 70 °C for 30 min and washed with water and ethanol.³⁹

Dye-Sensitized Solar Cell Fabrication. The 3D host–passivation–guest photoanodes are sintered for 30 min at 500 °C before dipping in a 0.3 mM Z907 solution (90 vol% 1:1 acetonitrile/tert-butanol, 10 vol% DMF) for 10 min. Following the immersion procedure, the dye-sensitized electrodes are rinsed with acetonitrile and dried in air. The photoanodes are then assembled using a thermally platinized FTO counter electrode (fabricated by spreading out a drop of 5 mM H₂PtCl₆ isopropanol solution on the FTO before treating it at 420 °C for 15 min) using a 25 μm thick hot melt ring (Surlyn, DuPont) and sealed by heating. The cell internal space was filled with a volatile I₃⁻/I⁻ electrolyte (1.0 M DMII, 0.03 M I₂, 0.5 M TBP, 0.05 M LiI, 0.1 M GuNCS), in a 85:15 acetonitrile/valeronitrile mixture through a predrilled hole using a vacuum pump.

Mobility Measurement on Al/ZnO and SnO₂. Electron mobility in Al/ZnO and SnO₂ was obtained using Hall Effect measurement (Microworld HMS-3000) on a 90 nm thick film on glass substrate at room temperature in the dark.

J-V Measurements. A 450 W xenon lamp (Oriel, U.S.A.) was used to provide an incident irradiance of 100 mW/cm² at the surface of the solar cells. The spectral output of the lamp was filtered using Schott K113 Tempax sunlight filter (Präzisions Glas & Optik GmbH, Germany) to reduce light mismatch between AM 1.5G and the simulated illumination to less than 2%.⁴⁷ J–V measurements were taken using a Keithley 2400 sourcemeter (Keithley, U.S.A.) by independently applying external voltage to the cell and measuring the photogenerated current. The size of the mask used to test the cells was 0.25 cm².

Scanning Electron Microscopy. Film morphology was investigated using a high-resolution scanning electron microscope (LEO 1550, Zeiss) equipped with a GEMINI column and a Schottky Field Emission source. Images were acquired using an In-Lens Secondary Electron Detector.

■ ASSOCIATED CONTENT

● **Supporting Information.** Additional table and figures. This material is available free of charge via the Internet at <http://pubs.acs.org>.

■ AUTHOR INFORMATION

Corresponding Author

*E-mail: (N.T.) nicolas.tetreault@epfl.ch; (G.A.O.) gozin@chem.utoronto.ca.

■ ACKNOWLEDGMENT

N.T. wishes to thank Dr. Morgan Stefk for the XRD of SnO₂. Research at EPFL was supported by the King Abdullah University of Science and Technology (KAUST, Award No KUS-C1-015-21). J.B. received financial support from a Marie Curie Research Training Network, Hydrogen Project (MRTN-CT-2006-032474). L.-P. H. received financial support from the Swiss National Science Foundation (Grant 200020_125163). This work was partially supported by the European project MULTIPLAT (NMP4-SL-2009-228943). For research at University of Toronto, G.A.O. is deeply indebted to the Government of Canada for a Research Chair in Materials Chemistry and Nanochemistry enabling this research at University of Toronto. In addition, he thanks the Natural Sciences and Engineering Research Council (NSERC) of Canada and the NSERC Solar Network for strong and sustained financial support of this work. E.A. thanks NSERC for a graduate scholarship.

■ REFERENCES

- (1) Chiba, Y.; Islam, A.; Watanabe, Y.; Komiya, R.; Koide, N. *Jpn. J. Appl. Phys.* **2006**, 45, L638–L640.
- (2) Gao, F.; Wang, Y.; Shi, D.; Zhang, J.; Wang, M.; Jing, X. *J. Am. Chem. Soc.* **2008**, 130, 10720–10728.
- (3) Graetzel, M. *Prog. Photovoltaics* **2006**, 14, 429–442.
- (4) Dloczik, L.; Illeperuma, O.; Lauermann, I.; Peter, L.; Ponomarev, E.; Redmond, G.; Shaw, N.; Uhendorf, I. *J. Phys. Chem. B* **1997**, 101, 10281–10289.
- (5) Kopidakis, N.; Schiff, E.; Park, N.; van de Lagemaat, J.; Frank, A. *J. Phys. Chem. B* **2000**, 104, 3930–3936.
- (6) van de Lagemaat, J.; Zhu, K.; Benkstein, K. D.; Frank, A. *J. Inorg. Chim. Acta* **2008**, 361, 620–626.
- (7) Martinson, A. B. F.; Elam, J. W.; Liu, J.; Pellin, M. J.; Marks, T. J.; Hupp, J. T. *Nano Lett.* **2008**, 8, 2862–2866.

- (8) Abayev, I.; Zaban, A.; Fabregat-Santiago, F.; Bisquert, J. *J. Phys. Status Solidi A* **2003**, *196*, R4–R6.
- (9) Wang, Q.; Ito, S.; Graetzel, M.; Fabregat-Santiago, F.; Mora-Sero, I.; Bisquert, J.; Bessho, T.; Imai, H. *J. Phys. Chem. B* **2006**, *110*, 25210–25221.
- (10) Clifford, J. N.; Palomares, E.; Nazeeruddin, M. K.; Graetzel, M.; Durrant, J. R. *J. Phys. Chem. C* **2007**, *111*, 6561–6567.
- (11) Zhang, Z.; Chen, P.; Murakami, T. N.; Zakeeruddin, S. M.; Graetzel, M. *Adv. Funct. Mater.* **2008**, *18*, 341–346.
- (12) Snaith, H. J. *Adv. Funct. Mater.* **2010**, *20*, 13–19.
- (13) O'Regan, B.; Schwartz, D. T.; Zakeeruddin, S. M.; Gratzel, M. *Adv. Mater.* **2000**, *12*, 1263–1267.
- (14) Bach, U.; Lupo, D.; Comte, P.; Moser, J.-E.; Weissortel, F. *Nature* **1998**, *395*, 583–585.
- (15) Snaith, H. J.; Moule, A. J.; Klein, C.; Meerholz, K.; Friend, R. H.; Graetzel, M. *Nano Lett.* **2007**, *7*, 3372–3376.
- (16) Wang, M.; Liu, J.; Cevey-Ha, N.; Moon, S.-J.; Liska, P.; Humphry-Baker, R.; Moser, J.-E.; Gratzel, C.; Wang, P.; Zakeeruddin, S. M.; Graetzel, M. *Nano Today* **2010**, *5*, 169–174.
- (17) Cai, N.; Moon, S.-J.; Cevey-Ha, L.; Moehl, T.; Humphry-Baker, R.; Wang, P.; Zakeeruddin, S. M.; Graetzel, M. *Nano Lett.* **2011**, *11* (4), 1452–1456.
- (18) Barnes, P. R. F.; Liu, L.; Li, X.; Anderson, A. Y.; Kissnerwan, H.; Ghaddar, T. H.; Durrant, J. R.; O'Regan, B. C. *Nano Lett.* **2009**, *9*, 3532–3538.
- (19) Kopidakis, N.; Benkstein, K.; van de Lagemaat, J.; Frank, A. *J. Phys. Chem. B* **2003**, *107*, 11307–11315.
- (20) Nelson, J.; Haque, S.; Klug, D.; Durrant, J. *Phys. Rev. B* **2001**, *63*, 205321.
- (21) Snaith, H. J.; Humphry-Baker, R.; Chen, P.; Cesar, I.; Zakeeruddin, S. M.; Graetzel, M. *Nanotechnology* **2008**, *19*, 424003.
- (22) Law, M.; Greene, L.; Johnson, J.; Saykally, R.; Yang, P. *Nat. Mater.* **2005**, *4*, 455–459.
- (23) Martinson, A. B. F.; Elam, J. W.; Hupp, J. T.; Pellin, M. J. *Nano Lett.* **2007**, *7*, 2183–2187.
- (24) Mor, G.; Shankar, K.; Paulose, M.; Varghese, O.; Grimes, C. *Nano Lett.* **2006**, *6*, 215–218.
- (25) Chen, P.; Brillet, J.; Bala, H.; Wang, P.; Zakeeruddin, S. M.; Graetzel, M. *J. Mater. Chem.* **2009**, *19*, 5325–5328.
- (26) Tetreault, N.; Horváth, E.; Moehl, T.; Brillet, J.; Smajda, R.; Bungener, S.; Cai, N.; Wang, P.; Zakeeruddin, S. M.; Forró, L.; Magrez, A.; Graetzel, M. *ACS Nano* **2010**, *4*, 7644.
- (27) Green, A.; Palomares, E.; Haque, S. A.; Kroon, J.; Durrant, J. *J. Phys. Chem. B* **2005**, *109*, 12525–12533.
- (28) Kay, A.; Gratzel, M. *Chem. Mater.* **2002**, *14*, 2930–2935.
- (29) Ramasamy, E.; Lee, J. *J. Phys. Chem. C* **2010**, *114*, 22032–22037.
- (30) Yang, W.; Wan, F.; Chen, S.; Jiang, C. *Nanoscale Res. Lett.* **2009**, *4*, 1486–1492.
- (31) Prasittichai, C.; Hupp, J. T. *J. Phys. Chem. Lett.* **2010**, *1*, 1611–1615.
- (32) Snaith, H. J.; Ducati, C. *Nano Lett.* **2010**, *10*, 1259–1265.
- (33) Miguez, H.; Tetreault, N.; Yang, S.; Kitayev, V.; Ozin, G. A. *Adv. Mater.* **2003**, *15*, 597–600.
- (34) Tetreault, N.; Freymann, von, G.; Deubel, M.; Hermatschweiler, M.; Perez-Willard, F.; John, S.; Wegener, M.; Ozin, G. *Adv. Mater.* **2006**, *18*, 457.
- (35) Kim, H.; Lee, H.-B.-R.; Maeng, W. J. *Thin Solid Films* **2009**, *517*, 2563–2580.
- (36) Li, T. C.; Goes, M. S.; Fabregat-Santiago, F.; Bisquert, J.; Bueno, P. R.; Prasittichai, C.; Hupp, J. T.; Marks, T. J. *J. Phys. Chem. C* **2009**, *113*, 18385–18390.
- (37) Le Formal, F.; Tetreault, N.; Cornuz, M.; Moehl, T.; Graetzel, M.; Sivula, K. *Chem. Sci.* **2011**, *2*, 737–743.
- (38) Miguez, H.; Tetreault, N.; Hatton, B.; Yang, S.; Perovic, D.; Ozin, G. A. *Chem. Commun.* **2002**, 2736–2737.
- (39) Ito, S.; Murakami, T.; Comte, P.; Liska, P.; Gratzel, C. *Thin Solid Films* **2008**, *516*, 4613–4619.
- (40) Cao, Y.; Bai, Y.; Yu, Q.; Cheng, Y.; Liu, S.; Shi, D.; Gao, F.; Wang, P. *J. Phys. Chem. C* **2009**, *113*, 6290–6297.
- (41) O'Regan, B. C.; Durrant, J. R.; Sommeling, P. M.; Bakker, N. J. *J. Phys. Chem. C* **2007**, *111*, 14001–14010.
- (42) Martinson, A. B. F.; McGarrah, J.; Parpia, M.; Hupp, J. *Phys. Chem. Chem. Phys.* **2006**, *8*, 4655–4659.
- (43) Martinson, A. B. F.; Goes, M. S.; Fabregat-Santiago, F.; Bisquert, J.; Pellin, M. J.; Hupp, J. T. *J. Phys. Chem. A* **2009**, *113*, 4015–4021.
- (44) He, C.; Zheng, Z.; Tang, H.; Zhao, L.; Lu, F. *J. Phys. Chem. C* **2009**, *113*, 10322–10325.
- (45) Keis, K.; Magnusson, E.; Lindstrom, H.; Lindquist, S.; Hagfeldt, A. *Sol. Energy Mater. Sol. Cells* **2002**, *73*, 51–58.
- (46) Moser, J.-E.; Wolf, M.; Lenzmann, F.; Graetzel, M. *Z. Phys. Chem.* **1999**, *212*, 85–92.
- (47) Ito, S.; Matsui, H.; Okada, K.; Kusano, S.; Kitamura, T.; Wada, Y.; Yanagida, S. *Sol. Energy Mater. Sol. Cells* **2004**, *82*, 421–429.